Large-Gap Quantum Spin Hall Insulator in Single Layer Bismuth Monobromide Bi4Br4

ARTICLE *in* NANO LETTERS · MAY 2014

Impact Factor: 13.59 · DOI: 10.1021/nl501907g · Source: arXiv

Large-Gap Quantum Spin Hall Insulator in single layer bismuth monobromide Bi_4Br_4

Jin-Jian Zhou,[1,2] Wanxiang Feng,[1] Cheng-Cheng Liu,[1] Shan Guan,[1] and Yugui Yao[1,*]

[1]*School of Physics, Beijing Institute of Technology, Beijing 100081, China*
[2]*Institute of Physics, Chinese Academy of Sciences and Beijing National Laboratory for Condensed Matter Physics, Beijing 100190, China*

(Dated: May 19, 2014)

Quantum spin Hall (QSH) insulators have gapless topological edge states inside the bulk band gap, which can serve as dissipationless spin current channels protected by the time-reversal symmetry. The major challenge currently is to find suitable materials for this topological state. Here, we predict a new large-gap QSH insulator with bulk direct band gap of ∼0.18 eV, in single-layer Bi_4Br_4, which could be exfoliated from its three-dimensional bulk material due to the weakly-bonded layered structure. The band gap of single-layer Bi_4Br_4 is tunable via strain engineering, and the QSH phase is robust against external strain. In particular, because this material consists of special one-dimensional molecular chain as its basic building block, the single layer Bi_4Br_4 could be easily torn to ribbons with clean and atomically sharp edges, which are much desired for the observation and application of topological edge states. Our work thus provides a new promising material for experimental studies and practical applications of QSH effect.

PACS numbers: 73.22.-f, 73.43.-f, 71.70.Ej, 85.75.-d

Topological insulators (TIs) have generated a surge of interests recent years due to their rich physics and promising applications in spintronics and quantum computations [1, 2]. The concept of QSH insulators, also known as two-dimensional TIs, was first proposed in graphene [3]; however, later works demonstrated that the band gap opened by spin-orbit coupling (SOC) is extremely small (10^{-3} meV) such that the QSH effect can not be observed in present experimental conditions [4–6]. Up to now, the QSH effect is only experimentally verified in HgTe/CdTe [7] and InAs/GaSb [8] quantum wells, in which stringent conditions, *e.g.* ultrahigh-quality samples and ultralow temperature, are required due to their small bulk band gaps (on the order of meV). Therefore, the search for QSH insulators with large band gaps and characteristics of easy fabrication is a key step towards the future studies and applications of QSH effect.

Many efforts have been made to search for QSH insulators with large gap and stable structures, and a number of QSH insulators have been theoretically proposed, such as silicene [9], Bi(111) bilayer [10], chemically modified Sn [11] and Bi/Sb [12] honeycomb lattices, and $ZrTe_5$/$HfTe_5$ [13]. However, silicene has very small band gap, besides, an appropriate insulating substrate that can support the growth of silicene is still lacking; the Bi(111) bilayer can host sizable band gap, similar difficulty exists with the growth of the thin film material on a suitable substrate [14, 15]; the chemically modified Sn, Sb and Bi honeycomb lattices are also difficult for experimental access, especially for the precise control of adatom coverage. The most promising approach for fabricating QSH insulators may be by cleaving a chemically stable two-dimensional (2D) system from their van der Waals (vdW) layered three-dimensional (3D) matrix, just like graphene made by the scotch-tape method from graphite [16].

In this Letter, based on first-principles calculations we report a new large-gap QSH insulator in single-layer Bi_4Br_4 with bulk direct band gap of ∼0.18 eV. The band gap can be effectively tuned by uniaxial strains, and the QSH phase is robust against external strains. The 3D bulk Bi_4Br_4, previously known as n-type semiconductor [17], is a vdW layered compound, and its interlayer binding energy is comparable to other layered systems that have been successfully exfoliated, such as graphite and MoS_2; therefore, the single layer Bi_4Br_4 could be made via the mechanical exfoliation from the bulk form. Our phonon spectrum calculations further suggest that the freestanding single layer structure can be stable. In particular, the single layer Bi_4Br_4 has one-dimensional infinite molecular chain as its building block; therefore, it could be naturally torn to nano-ribbons with clean and atomically sharp edges, which are much desired for the observation of topological edge states or serving as ideal one-dimensional (1D) dissipationless conducting wires.

First-principles calculations are performed using the projector augmented wave method [18] implemented in the Vienna *ab initio* simulation package [19]. The generalized gradient approximation of Perdew-Burke-Ernzerhof (GGA-PBE) is used for the exchange correlation potential [20]. The structures are optimized employing the vdW corrections by the approach of Dion *et al.* [21, 22]. The experimental lattice parameters are used for the bulk system, and the same lattice parameters for single layer system (lattice constants a=13.064 Å, b=4.338 Å for Bi_4Br_4)[23, 24]. The ionic position are relaxed until force on each ion is less than 0.01 eV·Å^{-1}. The phonon spectrum is calculated using the PHONOPY code [25] through the DFPT approach [26] without SOC. The Maximally Localized Wannier Functions (MLWFs) for the p orbitals of Bi and Br atoms are constructed

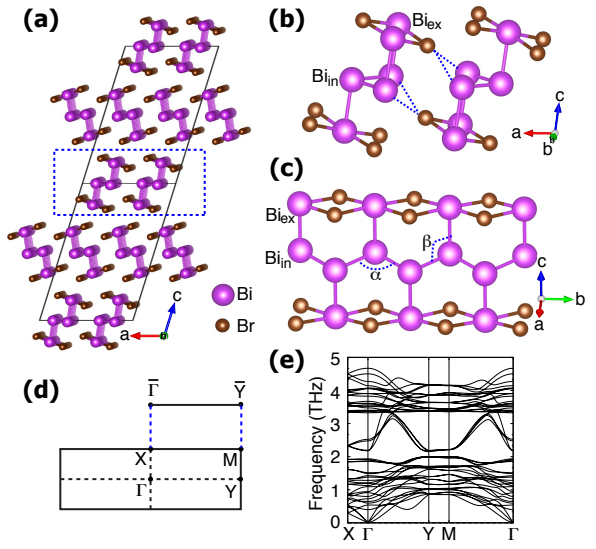

FIG. 1: (Color online) Crystal structure of Bi_4Br_4 in 3D (a), 2D (b), and 1D (c) representations. The large pink and small brown balls stand for Bi and Br atoms respectively. In the 1D chain, the Bi_{in} atoms in the middle form a zigzag chain, the Bi_{ex} atoms at the edge of the chain are bonded with Br atoms. (d) 2D and projected 1D Brillouin zones with high-symmetry points. (e) phonon spectrum of single layer Bi_4Br_4.

using the WANNIER90 code[27, 28]. Based on the generated MLWFs, a tight-binding model for ribbons are constructed to calculate the topological edge states.

Bulk Bi_4Br_4 crystallizes in the monoclinic space group $C2/m$ (C_{2h}^3) [23, 24]. Figure 1(a) shows the layered structure of bulk Bi_4Br_4, which can be regarded as a combined packing of the normal (marked by blue dash line) and mirror-reflected single layer along the c axis. In each 2D layer, as shown in Fig. 1(b), the basic building block is an 1D infinite molecular chain along the b axis. Figure 1(c) shows the structure of a single molecular chain. The middle Bi_{in} atoms form a zigzag chain with strongly covalent Bi_{in}-Bi_{in}bonds (∼3.0 Å), and the Br atoms are tightly attached to Bi_{ex} (∼2.9 Å) along the edges of the molecular chain. The Bi_{in}-Bi_{in} and Bi_{in}-Bi_{ex} bonds are nearly perpendicular to each other ($\alpha \sim 91°$, $\beta \sim 92°$). The bonds between Bi_{ex} and Br atoms in the adjacent chains [dash line in Fig. 1(b)] are relatively weak (∼3.6 Å). Despite the weak bonding between adjacent chains, the single-layer structure is rather stable, given that all the synthesized mixed bismuth monohalides $Bi_4Br_xI_{4-x}(x = 1, 2, 3)$ have the similar single-layer structure as Bi_4Br_4, while the inter-layer stacking patterns are diverse [24].

We have calculated the binding energy of the single-layer sheet to its bulk phase for Bi_4Br_4. The obtained value (∼20 meV/Å^2) is in the typical range for the vdW layered compounds [29]. Specifically, the binding energy of single layer Bi_4Br_4 is comparable to the experimental result of graphene(∼ 12 meV/Å^2)[30] , and slightly smaller than theoretical value of MoS_2 (∼26 meV/Å^2) in our calculations. This indicates that the experimental fabrication of single layer Bi_4Br_4 become possible using similar "scotch tape" method as that for graphene [16, 31] or MoS_2 [32, 33]. The dynamic stability of single layer Bi_4Br_4 is further investigated through the phonon spectrum calculations. The calculated phonon spectrum is shown in Fig. 1(e). The phonon frequencies are real at all momenta, which suggests a stable structure.

We now focus on the topological properties of electronic structure of single-layer Bi_4Br_4. For the convenience of discussion, hereafter all of calculations are based on a 2D conventional cell that includes two 1D chain units [see Fig. 1(b)]. The calculated band structure without SOC is plotted in Fig. 2(b), in which one can see that single layer Bi_4Br_4 is a semiconductor with direct band gap at the Γ point. From the view of density of states shown in Fig. 2(a), both of the valence and conduction bands near the Fermi level are mainly constituted by Bi-6p orbitals, The states below -2 eV are dominated by Br-4p orbitals due to the larger electronegativity of Br atoms. When SOC is switched on, the band gap maintains (∼0.35 eV) as shown in Fig. 2(c). To analyze the band topology, we have calculated the Z_2 topological invariant within the first-principle framework [34], based on the parity criterion proposed by Fu and Kane [35]. The result of Z_2=1 verifies that the single layer Bi_4Br_4 is a QSH insulator. It is well known that the GGA-type calculation may produce inaccurate band gap. To further confirm the nontrivial properties of our system, we have checked the band structure of Bi_4Br_4 using the more sophisticated Heyd-Scuseria-Ernzerhof hybrid functional method (HSE06) [36]. The resultant band is similar to the GGA result except a little smaller direct band gap (∼0.18 eV) at Γ-point, and the topological nontrivial phase remains unchanged.

The gapless chiral edge states inside the bulk band gap is the hallmark of QSH insulators. Because the coupling between the 1D molecular chains is much weaker than the intra-chain bonding [17], a natural nanoribbon can be easily constructed along the b-axis without any dangling bond. With the nanoribbon width of 40 chains (≈26 nm), the calculated band structure is presented in Fig. 2(d). One can see explicitly that the gapless edge states appear in bulk band gap cross linearly at the Γ point. The Fermi velocity of edge states in single layer Bi_4Br_4 is $\sim 4.8\times10^5$ m/s, which is slightly smaller than that of 5.5×10^5 m/s in HgTe/CdTe quantum well [2], but is remarkably larger than that of 3×10^4 m/s in InAs/GaSb quantum well [8]. This high Fermi velocity is beneficial to the fabrication of high-speed spintronics devices.

To elucidate the physical mechanism of the band inversion, we study the band structure evolution at Γ point, starting from the atomic orbitals. The schematic diagram of the evolution is plotted in Fig. 3(a). The 2D single layer Bi_4Br_4 cell consists of two 1D chains, and each chain has four Bi atoms and four Br atoms in a

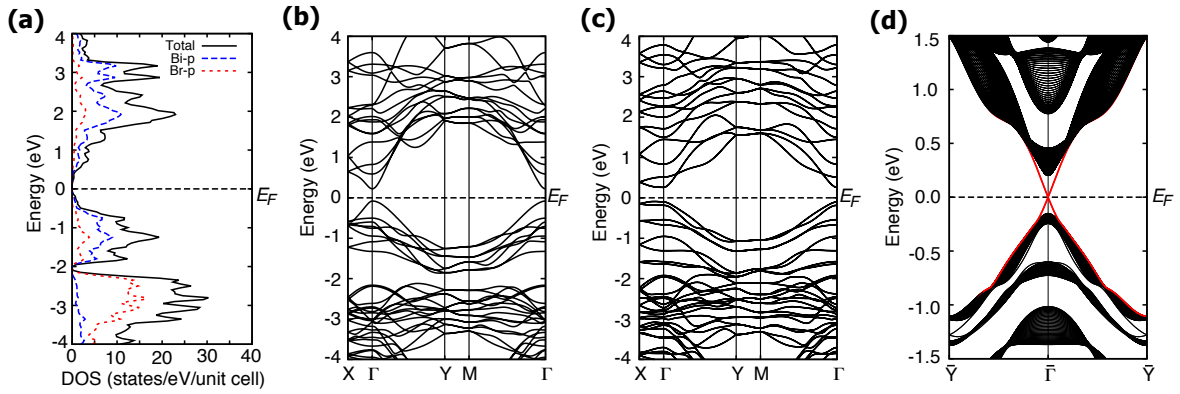

FIG. 2: (Color online) Density of states (a) and band structure (b) of single-layer Bi_4Br_4 without SOC. (c) Band structure when SOC is included. (d) Band structure of 1D nanoribbon edged along the molecular chain axis for Bi_4Br_4. Topological edge states are visualized by red lines crossing linearly at the Γ point, which indicates single-layer Bi_4Br_4 is a QSH insulator.

unit-cell. The Br-4p orbitals stay deep below the Fermi level due to the much larger electronegativity of Bromine. Therefore, it is reasonable to neglect the Br atoms, and only consider the Bi-6p orbitals. For clarity, the simplified structure with only Bi atoms is schematically plotted in Fig. 3(b).

We first consider the strongly covalent bonds within the 1D chain, and then take into account the weak inter-chain couping. For the 1D chain, the Bloch orbital at Γ point is given by $|p_\alpha\rangle = \sum_i p^i_\alpha$, where p^i_α $(\alpha = x, y, z)$ are the atomic orbitals in unit-cell R_i. At stage (1), mirror symmetry is considered. The structure has mirror symmetry with mirror plane parallel to xz plane. The $p_{x/z}$ and p_y orbitals at Γ point have different parities under mirror operation, hence they will not mix with each other (when SOC is absent). The p_y orbital has higher energy because of the much stronger σ-type hopping between p^i_y and p^{i+1}_y compared to the π-type of $p_{x/z}$. At stage (2), the inversion symmetry of the chain is considered. Under inversion operation, the two Bi_{in} (Bi_{ex}) atoms interchange site with each other. Orbitals from these two atoms can be combined to form bonding and anti-bonding states with splitted levels, which are given by

$$|Bi_{in/ex}, \alpha^{\pm}\rangle = \frac{1}{\sqrt{2}}(|Bi^1_{in/ex}, \alpha\rangle \mp |Bi^2_{in/ex}, \alpha\rangle)$$

with $\alpha = p_x, p_y, p_z$. They have definite parities as denoted in the upper index $\pm$. Only those states with the same parity can further couple with each other. We discuss the intra-chain bonding induced coupling between those states as following: (1) The splitting energy ΔE_x between $|\mathrm{Bi}_{in}, p^+_x\rangle$ and $|\mathrm{Bi}_{in}, p^-_x\rangle$ is quite large due to the short Bi_{in}-Bi_{in} bond length, so does the $|\mathrm{Bi}_{in}, p^\pm_y\rangle$. In addition, the relative size of ΔE_x and ΔE_y depends on the angle θ [see Fig. 3(b)]. The $p_x(p_y)$ orbital hopping t_{xx} (t_{yy}) between the two Bi_{in} atoms, which determine the ΔE_x (ΔE_y), is related to θ, namely, t_{xx} (t_{yy}) can be given by $t_{pp\sigma}\sin\theta^2 + t_{pp\pi}\cos\theta^2$ $(t_{pp\sigma}\cos\theta^2 + t_{pp\pi}\sin\theta^2)$. Therefore, the reduction of θ will decrease the ΔE_x and increase the ΔE_y. (2) The orbital hopping between the two Bi_{ex} atoms, which locate at different sides of the chain, is negligible. However, $|\mathrm{Bi}_{ex}, p^\pm_{x/y}\rangle$ can be coupled to $|\mathrm{Bi}_{in}, p^\pm_{x/y}\rangle$ through the $\pi-$bonding of $p_{x/y}$ orbital between Bi_{in}-Bi_{ex} atoms, which shifts $|\mathrm{Bi}_{ex}, p^+_{x/y}\rangle$ upward and $|\mathrm{Bi}_{ex}, p^-_{x/y}\rangle$ downward. (3) Due to the strong $\sigma-$bonding of p_z orbital between Bi_{in}-Bi_{ex} atoms, $|\mathrm{Bi}_{ex}, p^\pm_z\rangle$ mix with $|\mathrm{Bi}_{in}, p^\pm_z\rangle$ and splits into $|\mathrm{B1}, p^\pm_z\rangle$ and $|\mathrm{B2}, p^\pm_z\rangle$ states.

So far, we have considered all the intra-chain bonding. At stage (3), we start to count in the inter-chain coupling. The inter-chain coupling is dominated by the hopping between p_x orbitals because their orientations are parallel to the inter-chain direction. The $p^\pm_x$ orbitals from two adjacent chains (labeled as A, B) within the 2D cell are further splitted into bonding and anti-bonding states, for example

$$|Bi_{in/ex}, p^+_x, \pm\rangle = \frac{1}{\sqrt{2}}(|Bi^A_{in/ex}, p^+_x\rangle \mp |Bi^B_{in/ex}, p^+_x\rangle)$$

At final stage (4), the SOC is considered. The SOC mixes the orbital and spin with total angular momentum conserved, which results in the level repulsion between $|\mathrm{Bi}_{in/ex}, p^\pm_x\rangle$ and $|\mathrm{Bi}_{in/ex}, p^\pm_y\rangle$ [37], thus push the $|\mathrm{Bi}_{ex}, p^-_x, +\rangle$ downward and the $|\mathrm{Bi}_{in}, p^+_x, -\rangle$ upward, as shown in Fig. 3(a). Consequently, the band order is inverted (marked by the red dashed box). We show the Bi_{in}-p_x and Bi_{ex}-p_x orbitals projected bands in Fig. 3(c) (without SOC) and Fig. 3(d) (with SOC). As we can seen, in the absence of SOC, the valence band maximum(VBM) is dominated by the Bi_{in}-p_x orbital with negative parity, while the conduction band minimum (CBM) is dominated by the Bi_{ex}-p_x orbital with positive parity. After SOC is turned on, both the orbital character and the parity of CBM and VBM are inverted.

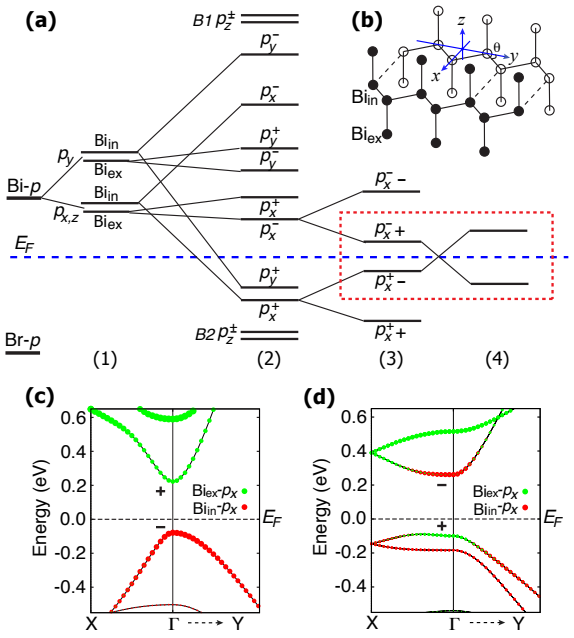

FIG. 3: (Color online) (a) Schematic diagram of the band evolution at Γ-point. The evolution stages are explained in the main text. (b) Schematic figure of the single layer Bi_4Br_4 structure with Br-atoms neglected. The filled and empty circles stand for Bi-atoms from adjacent chains. The solid lines denote strong intra-chain bonds, the dash lines denote weak inter-chain coupling. The Bi_{in}-p_x and Bi_{ex}-p_x orbital projected character of bands without (c) and with (d) SOC, the parity is labeled for CBM and VBM at Γ-point.

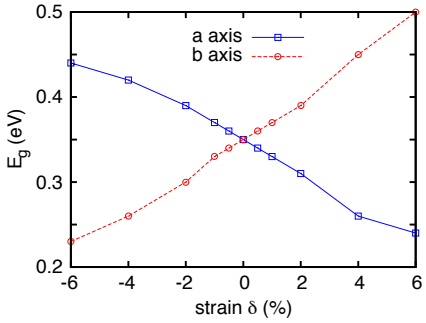

FIG. 4: (Color online) Band gaps of single layer Bi_4Br_4 as a function of uniaxial strains.

Application of external strain can effectively modify the band gap of single layer Bi_4Br_4, as shown in Fig. 4. Due to the structural anisotropy, we adopt separately the uniaxial strains along a- and b-axises. The change of band gap under the uniaxial strains displays a opposite behavior, i.e. increasing the lattice constant a will diminish the band gap, while increasing the lattice constant b will enlarge the band gap. This behavior can be understood from the above band evolution analysis. Increasing a will extend the inter-chain distance, which decreases the inter-chain coupling. The weakened inter-chain coupling will diminish the splitting at stage (3) in Fig. 3(a) and decrease the band gap ultimately. As we increase the lattice constant b, the angle θ becomes smaller accordingly while the Bi_{in}-Bi_{in} bond length hardly changes. With smaller θ, the $|\mathrm{Bi}_{in}, p_x^+\rangle$ will move upward to reduce the splitting [stage 2 in Fig. 3(a)], which then enlarges the band gap ultimately. Although the band gap can be effectively tunned by external strain, The topological nontrivial phase survives in a large range of strains from -6% to 6%, indicating the high stability of the QSH state.

Finally, we extend our discussion to the multilayer structures of Bi_4Br_4. Usually, when the single-layers are stacked together to form a multilayer film or 3D compound, the band gap will be reduced due to the inter-layer orbital hopping. In our systems, the inter-layer coupling is rather weak and the band edges are all dominated by the in-plane orbitals; therefore, we do not expect much band gap reduction in multilayer Bi_4Br_4 compared to the single layer one. Even for the 3D compound, the inverted band gap (∼0.15 eV) is only reduced by ∼30 meV according to our HSE06 calculations. Therefore, The inverted band gap should survive in multilayer Bi_4Br_4, and the Z_2 topological order would exhibit an interesting even-odd oscillation with increasing number of layers [38], which means those ultra-thin films with odd number of layers are QSH insulators as well. This will make the fabrications of QSH insulators in 2D Bi_4Br_4 systems much more flexible. We have also investigated another bismuth monohalides Bi_4I_4, which has the similar structure as Bi_4Br_4 [23, 24]. The single layer Bi_4I_4 is near the boundary of topological trivial and nontrivial phase transition; hence its QSH phase can be effectively tuned by uniaxial strains. In summary, the 2D Bi_4Br_4 is the most promising QSH insulator with large band gap (∼0.18 eV) and the advantage of easy fabrication. The Bi_4Br_4 nanoribbon can serve as an ideal 1D wire for dissipationless transport, or be utilized to create and manipulate majorana fermion via, e.g. putting the nanoribbon on the s-wave superconductors with external magnetic fields [39].

This work was supported by the MOST Project of China (Nos. 2014CB920903, 2013CB921903, 2011CBA00100), the NSF of China (Nos. 11174337, 11225418, 11374033) and the SRFDPHE of China (No. 20121101110046, 20131101120052).

* Electronic address: ygyao@bit.edu.cn

[1] M. Z. Hasan and C. L. Kane, Rev. Mod. Phys. **82**, 3045 (2010).
[2] X.-L. Qi and S.-C. Zhang, Rev. Mod. Phys. **83**, 1057 (2011).
[3] C. L. Kane and E. J. Mele, Phys. Rev. Lett. **95**, 226801 (2005).
[4] Y. G. Yao, F. Ye, X. L. Qi, S.-C. Zhang, and Z. Fang,

Phys. Rev. B **75**, 041401(R) (2007);
[5] D. Huertas-Hernando, F. Guinea and A. Brataas, Phys. Rev. B **74**, 155426 (2006).
[6] H. Min, J. E. Hill, N. A. Sinitsyn, B. R. Sahu, L. Kleinman, and A. H. MacDonald, Phys. Rev. B **74**, 165310 (2006).
[7] M. König, S. Wiedmann, C. Brüne, A. Roth, H. Buhmann, L. W. Molenkamp, X. L. Qi, and S.-C. Zhang, Science **318**, 766 (2007).
[8] I. Knez, R. R. Du, and G. Sullivan, Phys. Rev. Lett. **107**, 136603 (2011).
[9] C.-C. Liu, W. X. Feng, and Y. G. Yao, Phys. Rev. Lett. **107**, 076802 (2011); C.-C. Liu, H. Jiang, and Y. G. Yao, Phys. Rev. B **84**, 195430 (2011).
[10] S. Murakami, Phys. Rev. Lett. **97**, 236805 (2006).
[11] Y. Xu, B. H. Yan, H. J. Zhang, J. Wang, G. Xu, P. Z. Tang, W. H. Duan, and S.-C. Zhang, Phys. Rev. Lett. **111**, 136804 (2013).
[12] Z. Song, C.-C. Liu, J. Yang, J. Han, M. Ye, B. Fu, Y. Yang, Q. Niu, J. Lu, and Y. G. Yao, arXiv: 1402.2399 (2014); C.-C. Liu, S. Guan, Z. Song, S. A. Yang, J. Yang, and Y. G. Yao, arXiv:1402.5817 (2014).
[13] H. M. Weng, X. Dai, and Z. Fang, Physical Review X **4**, 011002 (2014).
[14] T. Hirahara, G. Bihlmayer, Y. Sakamoto, M. Yamada, H. Miyazaki, S. I. Kimura, S. Blügel, and S. Hasegawa, Phys. Rev. Lett. **107**, 166801 (2011).
[15] F. Yang, L. Miao, Z. F. Wang, M.-Y. Yao, F. Zhu, Y. R. Song, M.-X. Wang, J.-P. Xu, A. V. Fedorov, Z. Sun, G. B. Zhang, C. Liu, F. Liu, D. Qian, C. L. Gao, and J.-F. Jia, Phys. Rev. Lett. **109**, 016801 (2012).
[16] K. S. Novoselov, A. K. Geim, S. V. Morozov, D. Jiang, Y. Zhang, S. V. Dubonos, I. V. Grigorieva, and A. A. Firsov, Electric Field Effect in Atomically Thin Carbon Films, Science **306**, 666 (2004).
[17] T. G. Filatovaa, P. V. Gurinb, L. Klooc, V. A. Kulbachinskiib, A. N. Kuznetsova, V. G. Kytinb, M. Lindsjoc, B. A. Popovkina, J. Solid State Chem. **180**, 1103 (2007).
[18] P. E. Blöchl, Phys. Rev. B **50**, 17953 (1994).
[19] G. Kresse and J. Hafner, Phys. Rev. B **48**, 13115 (1993); G. Kresse and J. Furthmuller, Phys. Rev. B **54**, 11169 (1996).
[20] J. P. Perdew, K. Burke, and M. Ernzerhof, Phys. Rev. Lett. **77**, 3865 (1996).
[21] M. Dion, H. Rydberg, E. Schröder, D. C. Langreth, and B. I. Lundqvist, Phys. Rev. Lett. **92**, 246401 (2004).
[22] J. Klimeš, D. R. Bowler, and A. Michaelides, Phys. Rev. B **83**, 195131 (2011).
[23] H. von Benda, A. Simon, and W. Bauhofer, Z. Anorg. Allg. Chem., **438**, 53 (1978).
[24] E. V. Dikarev, B. A. Popovkin, and A. V. Shevelkov, Russ. Chem. Bull. Int. Ed., **50**, 2304 (2001).
[25] A. Togo, F. Oba, and I. Tanaka, Phys. Rev. B **78**, 134106 (2008).
[26] X. Gonze and C. Lee, Phys. Rev. B **55**, 10355 (1997).
[27] N. Marzari and D. Vanderbilt, Phys. Rev. B **56**, 12847 (1997); I. Souza, N. Marzari, and D. Vanderbilt, Phys. Rev. B **65**, 035109 (2001).
[28] A. A. Mostofi, J. R. Yates, Y.-S. Lee, I. Souza, D. Vanderbilt, and N. Marzari, Comp. Phys. Comm. **178**, 685 (2008).
[29] T. Björkman, A. Gulans, A. V. Krasheninnikov, and R. M. Nieminen, Phys. Rev. Lett. 108, 235502 (2012).
[30] Z. Liu, J. Z. Liu, Y. Cheng, Z. Li, L. Wang, and Q. Zheng, Phys. Rev. B **85**, 205418 (2012).
[31] A. K. Geim and K. S. Novoselov, Nat. Mater. **6**, 183 (2007).
[32] K. S. Novoselov, D. Jiang, F. Schedin, T. J. Booth, V. V. Khotkevich, S. V. Morozov, and A. K. Geim, Proc. Natl. Acad. Sci. U.S.A. **102**, 10451 (2005).
[33] B. Radisavljevic, A. Radenovic, J. Brivio, V. Giacometti, and A. Kis, Nat. Nanotech. **6**, 147 (2011).
[34] W. X. Feng, J. Wen, J.-J. Zhou, D. Xiao, and Y. G. Yao, Comp. Phys. Comm. **183**, 1849 (2012).
[35] L. Fu and C. L. Kane, Phys. Rev. B **76**, 045302 (2007).
[36] J. Heyd, G. E. Scuseria, and M.Ernzerhof, J. Chem. Phys. **118**, 8207 (2003); J. Chem. Phys. **124**, 219906 (2006).
[37] C.-X. Liu, X.-L. Qi, H. J. Zhang, X. Dai, Z. Fang, and S.-C. Zhang, Phys. Rev. B **82**, 045122 (2010).
[38] B. Yan, L. Müchler, and C. Felser, Phys. Rev. Lett. **109**, 116406 (2012).
[39] J. Alicea, Rep. Prog. Phys. **75**, 076501 (2012).